# Experimental Study of a Low-Speed Single Circular Jet Flow using Particle Image Velocimetry

**Lingges Shaswat**

**19th December 2023**

## Abstract

*This experimental study delves into the intricate dynamics of turbulent flow from a single circular jet, utilising PIV in a low-speed recirculating water tunnel. The experiment integrates a laser and a high-speed camera in a water tunnel that captures velocity field data crucial for analysing the flow characteristics. The circular jet unveils distinctive flow patterns, shear layer instabilities and vortex formations. The mean streamwise velocity experiences decay as the jet progresses downstream and spreads radially outward. The flow investigated has a Reynolds number of 2240, exhibiting both laminar and turbulent states. The momentum distribution was shown by the Reynolds shear stress analysis, and it accentuates the effects of shear layer instabilities. Vorticity patterns reveal the dynamic behaviour of fluid motion while an assessment of turbulent kinetic energy highlights higher turbulence levels within shear layer regions. This study aims to provide a comprehensive review of the dynamics of turbulent flows.*

## 1. Introduction

The study of turbulent flows has evolved throughout the years, incorporating theoretical, experimental, and computational methodologies. These comprehensive investigations are critical across scientific and engineering disciplines in optimising the design and efficiency of various systems by understanding the behaviour of fluid flow. Researchers delve into this realm of fluid mechanics, to seek insights into how turbulence impacts processes such as heat, mass, and momentum transfer. Despite extensive experimental studies on turbulent jet flows, several aspects remain unexplored due to the challenges associated with accurately predicting the interaction of flow structures. In an AGARD report, Ball et al. concluded (Fellouah, Ball and Pollard, 2009):

*"...Progress in turbulence modelling and simulation has been hampered by the lack of well documented, systematically verified, experimental and numerical databases of relatively simple building block flows for the validation of computational methods."*

This statement remains true until today. The fundamental interest in exploring these flows is generated by free jets which have been thoroughly explored due to their growing significance in many modern engineering applications.

Circular jets represent fundamental fluid configurations as they span many integral applications as a free shear flow due to the axisymmetric configuration. The dynamics of the fluid flow can lead to the creation of flow patterns, wakes and mixing layers. Shear layer vortices are associated with turbulence and are important for understanding fluid flow behaviours as shown in Figure 1. Many studies show fluid flow patterns such as Becker and Massaro as they showed the evolution of vortices and shear layer instabilities from an asymmetrical jet (Becker and Massaro, 1968). In addition, they established a linear relationship between the frequency of shear layer vortices with the square root of the flow's Reynolds number. Bradshaw investigated that the shear layer instability of a circular free jet is affected by the thickness of the initial boundary layer (Bradshaw, 1966). Unforced jets were studied by Crow and Champagne over a broad range of Reynolds numbers and were seen to have orderly structures – formation of shear layer vortices (Crow and Champagne, 1971). Through extensive research, it has been widely acknowledged that velocity gradients existing within the shear layer of a free jet led to the formation of shear layer vortices (Zang and New, 2015). The general jet response was investigated by Hussain and Zaman when controlled excitation, function of Strouhal number, formed rolled-up

vortex pairs (Z A M A N And, 1980). The outcomes presented by Fellouah et al. revealed a pronounced correlation between the mean velocity distribution and the turbulence intensities (Fellouah, Ball and Pollard, 2009). There are numerous research articles on characterising and understanding the turbulent flow structures as mentioned above.

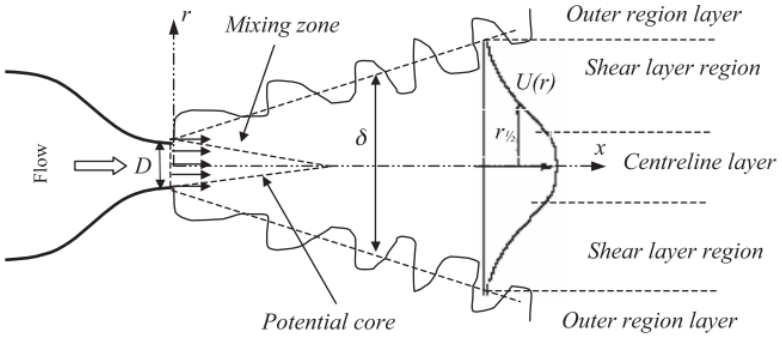


**Fig 1:** Schematic of a circular jet with discretised flow regions (Fellouah, Ball and Pollard, 2009).

There are various experimental techniques to capture turbulent flows such as Hot Wire Anemometry (HWA), Laser Doppler Velocimetry (LDV) and Particle Image Velocimetry (PIV). PIV has been used extensively in experimental fluid mechanics and has contributed to our extensive knowledge of turbulent flows. PIV is a non-intrusive technique that provides detailed information about how fluids move and interact by recording the velocity of the tracking particles that are illuminated by a laser that are suspended in a fluid. In the near-field region of the jet, the initial velocity profiles and their associated fluctuations can be readily determined from PIV, which encompasses turbulent kinetic energy and Reynolds shear stress. The main benefit the PIV has over its counterparts is that it produces vector fields in both 2D and 3D, while the other methods measure velocity at a point. PIV has progressed through the years and now it is routinely applied in aerodynamic research. Balachander et al demonstrated that PIV can be applied to complex turbulent water flows by comparing instantaneous flow fields and the effects of time resolution (Hyun, Balachandar and Yu, 2014).

This report focuses on a comprehensive analysis of flow characteristics from a circular jet using PIV by employing statistical methods which can then be a basis for understanding low-speed turbulent flows as there is not much literature published.

## 2. Methodology

*2.1 Experimental Setup*

The experiment was conducted in a low-speed recirculating water tunnel with internal dimensions measuring 450 $mm$ (width) x 600 $mm$ (height) x 1100 $mm$ (length) and was uniformly seeded with 55 $\mu m$, 1.03 $g/cm^3$ polyamide tracing particles as shown in Figure 2. The room where this experiment was conducted had to be dim as the particles illuminate when the laser is switched on. The tempered glass construction of the test region allowed for good optical access from both sides and the bottom. A water supply system was created using an additional smaller water tank placed above the water tunnel. This tank facilitated the delivery of the single circular jet at the top of the water tunnel which is essential in this experiment. The water flow was channelled from the back of the water tunnel through a centrifugal pump into the central compartment of the overhead tank which directed the jet into the water tunnel test region. This design aimed to minimize additional disturbances originating from the pump. The circular jet was submerged but positioned above and at the centre of the water tunnel and was measured to have an internal diameter ($D$) of 20 $mm$. Honeycomb structures were used to keep the flow laminar and eliminate crossflow disturbances. The temperature was kept constant at 20°$C$ to minimise temperature fluctuation effects. The jet flow was maintained at a mean exit velocity of $U = 0.122\ m/s$ and was measured by needle valves and monitored by Flotech iSOLV electromagnetic flowmeters with a measurement error of $\pm 0.5\%$. The coordinate system is defined

as $x$ and $y$ in the streamwise and cross-stream directions respectively. The origin is set at the exit of the jet centre.

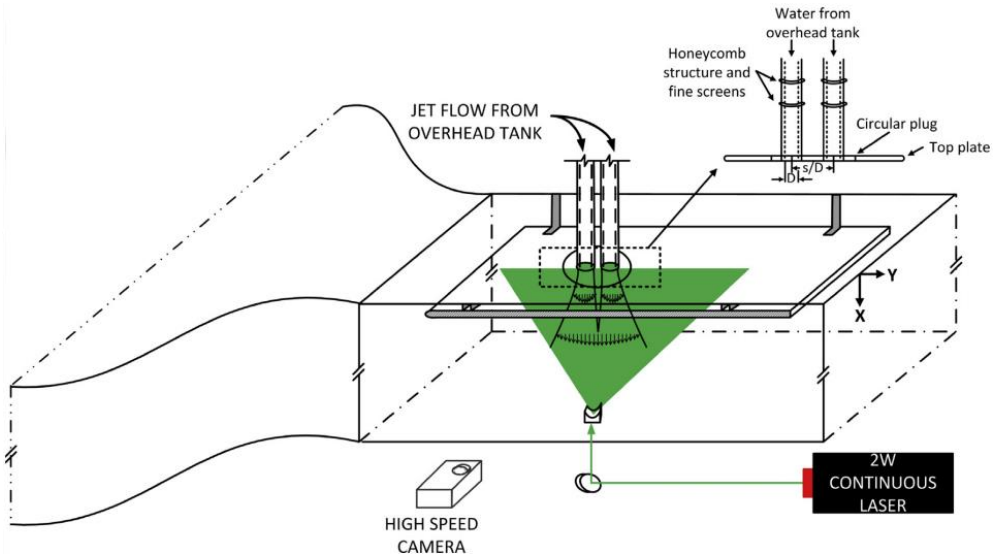


**Fig 2:** Similar Experimental PIV Setup shown for two jets with coordinate system labelled (Zang and New, 2015).

*2.2 Hardware Selection*

An illumination source was provided by a $2W$ CNI diode-pumped solid-state (DPSS) laser with a wavelength of 532 $nm$. The laser, operating in continuous wave (CW) mode, was equipped with beam-steering and sheet-forming optics to generate a thin laser sheet of approximately 1.5 $mm$ thickness. The laser was placed at the transparent test section floor outside of the water tunnel and aligned precisely with the jet flow centreline.

The scattered light reflections from polyamide seeding particles, within the jet flows and water tunnel were captured by a high-speed LuftvisCam-150 camera. The camera, with a resolution of 640×480, operated at a rate of 150 frames per second. The centrifugal compressor had a power rating of $370W$ to direct the jet into the test region. The experiment apparatus is shown in **Figure 3**.


(a) (b) (c)

**Fig 3:** Experimental apparatus includes (a) a high-speed Luftvis Cam-150 camera, (b) a centrifugal compressor and (c) a continuous wave laser rated 2W.

*2.3 Data Collection and Post-Processing*

The high-speed camera was placed normal to the jet flow centreline and was used to capture 1001 time-sequenced images in the $xy$ measurement plane at 15 frames per second. Calibration was done by inserting a ruler in line with the laser sheet. These raw images were then processed by a software

called PIVLab. This inter-frame time was found to have no more than 10 pixels shift of the final PIV interrogation window size and the uncertainty was expected to be 1%. The instantaneous velocity vector fields were obtained by subjecting pairs of consecutive images to multi-grid cross-correlations with the final interrogation window size being 74×95 coupled with 75% of window overlap in the vertical and horizontal direction. This was used as it improves resolution and allows large particle pixel placements. Consequently, the local median validation technique was done on PIVLab to remove visibly wrong velocity vectors and were replaced by vectors that were linearly interpolated. The obtained data was exported to MATLAB. This investigation acknowledges the experimental uncertainty associated with the measured velocity vectors as it is anticipated to be $\pm 1\%$ according to the guidelines from Keane and Adrian (Keane and Adrian, 1992).

*2.4 System Errors*

Various systematic errors are due to the setup, the recording process, and the evaluation methods. The alignment of the laser sheet with the streamwise flow direction is crucial to ensure proper data collection. Perspective errors become more apparent when the distance from the camera to the measurement plane increases or lens distortion which affects the velocity vectors. Calibration errors also occur if the laser sheet is too thick or if the camera does not coincide with the plane of interest. Errors due to the apparatus required in the experiment also have to be considered, such as the pulse delay of the laser. Flow that has large velocity gradients will be susceptible to errors due to the particle slip (Raffel *et al.*, 2018). Particle velocity lag should be accounted for, as the seeding density affects the spatial distribution, to ensure an accurate representation of experimental results.

## 3. Results and Discussion

*3.1 Reynolds Number*

The Reynolds number is a ratio of inertial forces to viscous forces. This dimensionless quantity is essential as it helps determine the type of fluid flow and predict the transition of the flow from laminar to turbulent. The Reynolds number can be found by using Equation 1, $U$ is the free stream velocity of the flow, $D$ is the jet's diameter and $v$ is the kinematic viscosity of the fluid given to be 0.000001 $m^2/s$ .

$$Re = \frac{UD}{v} \tag{1}$$

The Reynolds number calculated for this flow is 2240 and was kept constant in this experiment with a free stream velocity ($U$) of 0.112 m/s. This shows that the flow is transient as it is between 2000 and 4000 (Shashi Menon, 2015). Laminar characteristics will dominate below this threshold leading to organised streamlines whereas beyond this point, the onset of turbulence is expected. This flow exhibits both behaviours at different streamwise locations and will be studied below.

*3.2 Velocity*

The mean streamwise velocity from the single circular jet is shown in Figure 4a to show the development of flow fields. As the flow moves downstream, the mean velocity decays as flow development occurs. This decay can be attributed to the spreading of the jet with the surrounding ambient fluid leading to a gradual dissipation of kinetic energy as momentum exchanges between the two adjacent fluid layers. The jet exit velocity is retained for a short distance ($x/D = 2$) as this is due to the absence of viscous effects in that region, known as the potential core. This is where the maximum mean streamwise velocity occurs. The decay of centreline velocity and radial spread was shown to increase as the Reynolds number increased as investigated by Abdel-Rahman et al (Abdel-Rahman, Al-Fahed and Chakroun, 1996). The observed flow patterns align with established experimental data from various works of literature (Gohil, Saha and Muralidhar, 2012; Zang and New, 2015; Rovira, Engvall and Duwig, 2020).

The normalised mean streamwise velocity is shown in Figure 4b to show the decrease in the mean velocity in the radial direction from the centre of the jet in an axisymmetric manner. The width of the velocity profile can show the jet spread expands outward because of jet entrainment. From $x/D = 1$ to $x/D = 3$, the normalised velocity reduced less than from $x/D = 4$ to $x/D = 6$ and this can be seen in Figure 4a, as it is still part of the length of the potential core. The decay rate of the mean streamwise centreline velocity at a lower Reynolds number was found to have higher levels of turbulence intensities according to Olsson and Fuchs (Olsson and Fuchs, 1996). Moreover, Kwon and Seo showed that as the Reynolds number increased, the length of the potential core reduced and the Reynolds shear stress levels increased (Seo and Kwon, 2004).

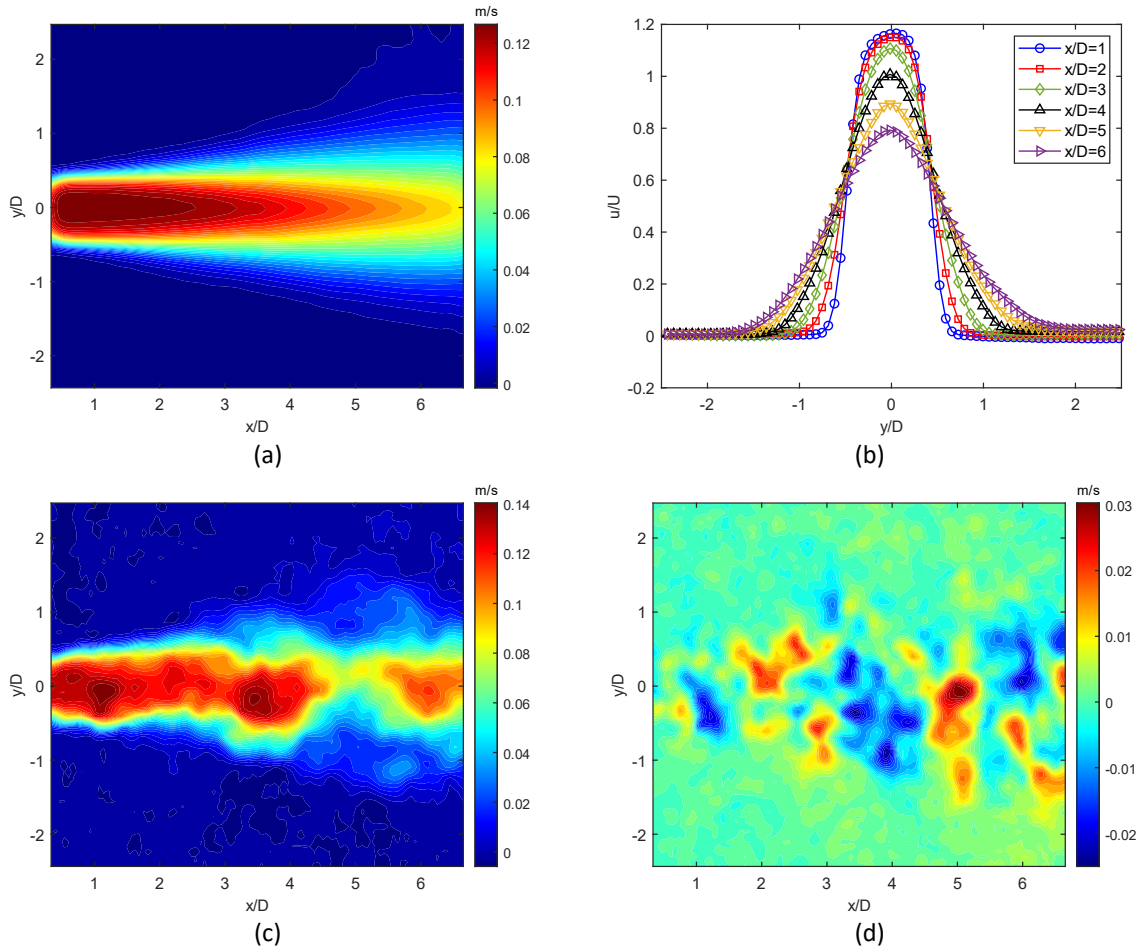


**Fig 4:** (a) The mean streamwise velocity profile and (b) the normalised mean streamwise velocity distributions at six different points downstream. At the first instant, (c) the streamwise and (d) the cross-stream velocity profiles are shown. Dimensionless time-averaged velocity (u/U*).

In the initial temporal snapshot, shown in Figure 4c and Figure 4d, the streamwise velocity at the near field of the jet dominates the cross-stream velocity as fluid is propagated from the jet. At $x/D = 5$, the streamwise velocity reduces as cross-stream velocity increases indicating the start of the flow becoming turbulent as there are more interactions with the ambient fluid. This phenomenon shows that turbulent flow characteristics are due to the shear stresses the fluid layers have with each other.

*3.3 Reynolds Shear Stress*

Reynolds shear stresses are an important aspect as they provide insight into the distribution of momentum between fluid layers. The Reynolds shear stress was found by determining the covariance of the fluctuating velocities components, $u'$ and $v'$. As expected, at the jet centreline, there is no shear stress because there are no viscous effects due to the constant velocity. Figure 5a shows the profile of

shear stress and it can be seen at the axisymmetric jet centreline, the directions of the shear stress are opposites, so the vortices are rotating in opposite directions. In Figure 5b the shear stress was shown and is not symmetric with the radial distance from the jet axis and this shows the effect of random turbulence. The shear layers of the single jet are quite symmetric in the turbulence level but reduce as the flow propagates in the streamwise direction as the shear layer regions become turbulent. As within the shear layer, the vortex cores will form which will evolve far field and pair up to form larger eddies due to the large velocity gradient in the radial direction. The maximum Reynolds shear stress shifts away from the centreline with increasing downstream distance.

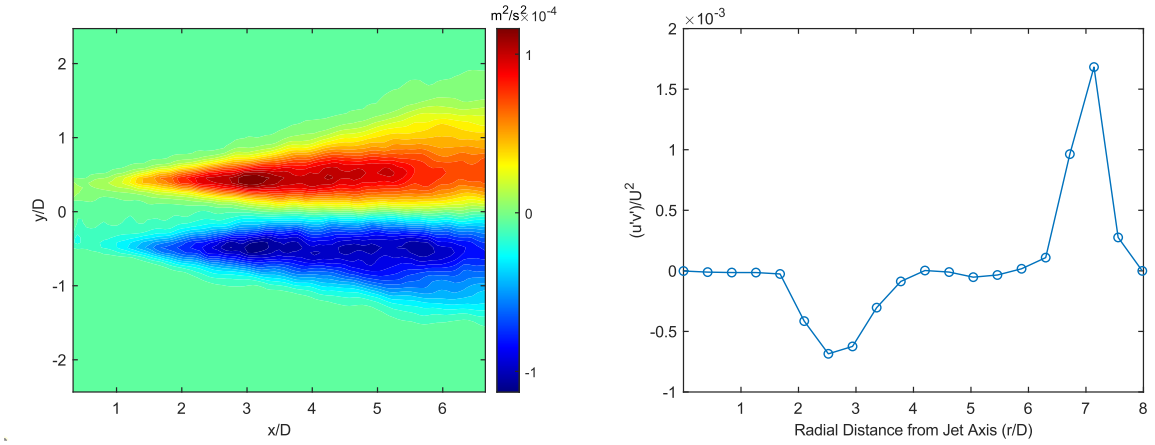


**Fig 5:** (a) The Reynolds shear stress profile and (b) the normalised mean Reynolds shear stress ($u'v'/U^2$) along the radial jet axis show the dynamics of turbulence.

### *3.4 Vorticity*

Vorticity patterns show the dynamic behaviour of fluid motion in terms of rotational motion and turbulence as they help characterise vortical structures which are essential in turbulent flow dynamics. At the first instant, shown in Figure 6a, vortex formations are evident near the jet nozzle as circular jets are susceptible to initial shear layer instabilities. The shear layer instability arises due to the difference in velocity between the jet exit and the ambient fluid and this is termed as the Kelvin-Helmholtz instability. This can lead to the formation of vortices and the creation of turbulent eddies which affect the characteristics of the flow. The mean vorticity is shown in Figure 6b and it is evident that the instability near the jet exit plays a significant part in creating vortices. The region deviates as the flow moves more downstream. The regions with high turbulence intensity correspond to the maximum of the mean velocity gradient (Fellouah, Ball and Pollard, 2009).

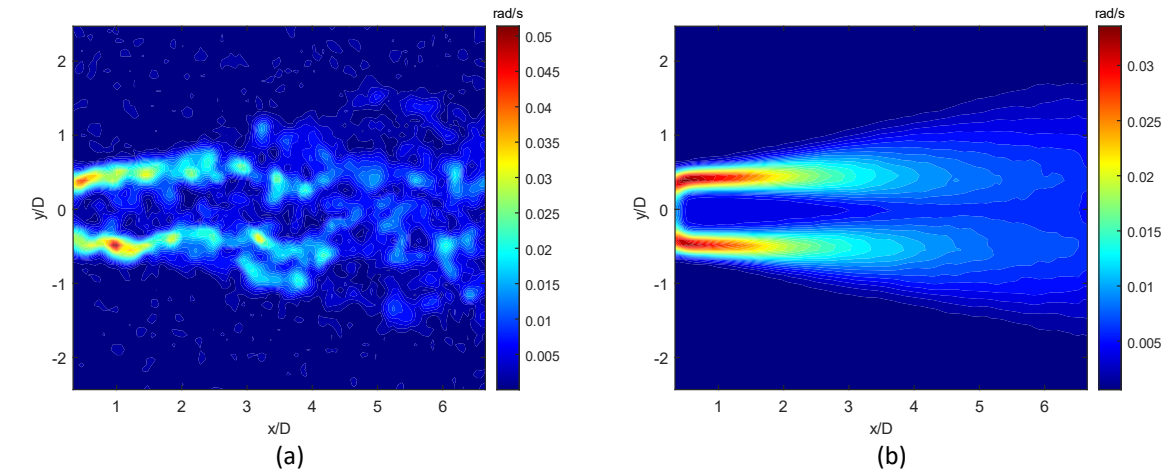

**Fig 6:** (a) Vorticity at the first instant shows that it is evident around the jet exit due to the difference in fluid velocities and (b) the mean vorticity profile of the jet flow.

### *3.5 Turbulent Kinetic Energy (TKE)*

TKE is a key parameter of turbulent flow study, as it represents the energy associated with eddies and the chaotic motion of fluid elements. The TKE was found by averaging the squared deviations (root mean squared) of the velocity components from their mean values. Figure 7a shows that there is less turbulence in the potential core region but higher turbulence in the shear layer regions. Since the jet is axisymmetric, it is evident that the shear layers are too. The potential core can be seen in Figure 7a as it ends at $x/D = 3$. Figure 7b shows the normalised TKE distribution in six downstream locations. As the flow moves downstream from the jet exit, the shear layers diminish and transit into turbulence which diminishes TKE levels. The turbulent flow is involved in a continuous transfer of energy and momentum, where larger eddies break down until the kinetic energy is dissipated as heat.

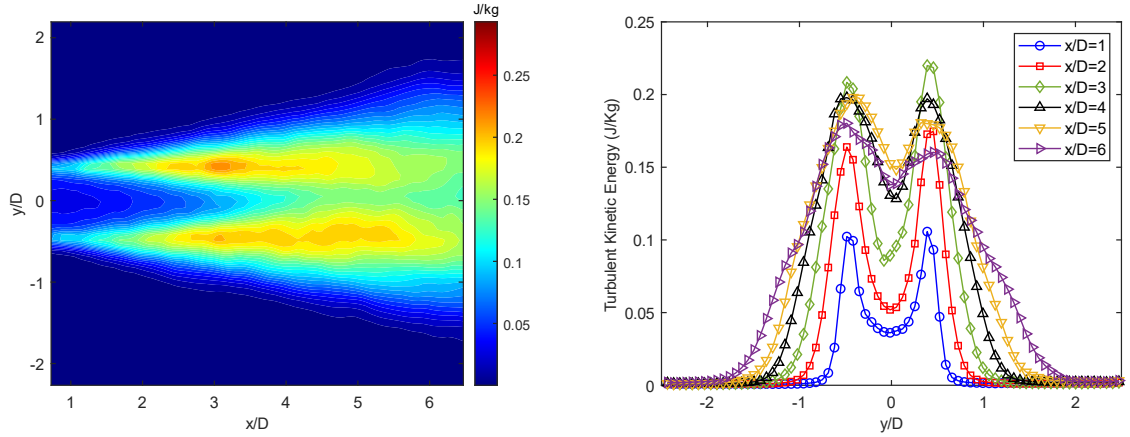


(a) (b)

**Fig 7:** (a) The mean TKE profile and (b) the normalised mean TKE distributions at six downstream locations.

### *3.6 Uncertainty Analysis*

Uncertainty analysis was found by a technique called bootstrapping as it is a resampling technique that is used when only one dataset is available due to factors that include complexity and cost which are substantial for PIV. A sample size of 10000 was taken to estimate the mean and the standard deviation as shown in Figure 8. The area of interest was at the maximum velocity of the flow which was at the centre of the jet nozzle. The mean streamwise velocity found was $0.131 \pm 0.00044\ m/s$ and the standard deviation was $0.0069 \pm 0.0003\ m/s$. The limitations of this method include the high sensitivity to the sample size and that the sampling distribution is the same for each observation.

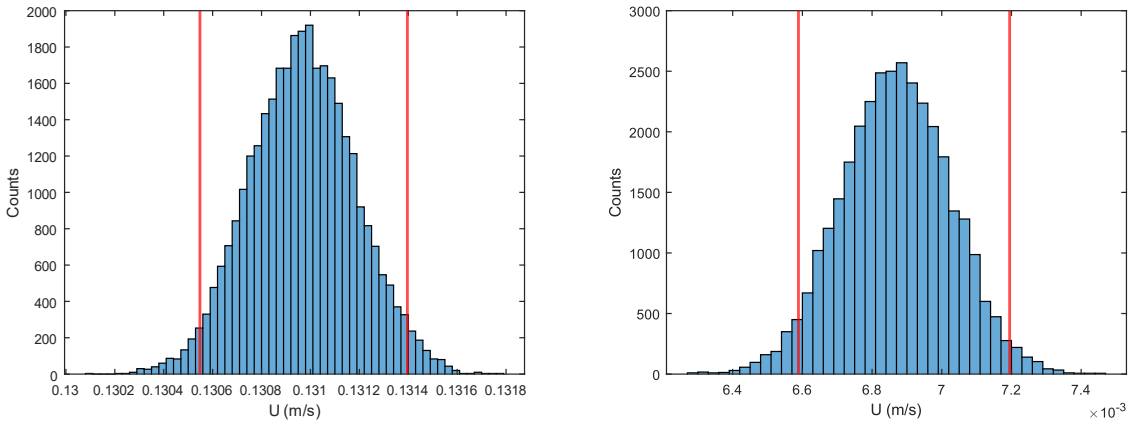


(a) (b)

**Fig 8:** Bootstrap distribution of the (a) mean streamwise velocity and (b) the standard deviation of streamwise velocity with a 95% confidence level labelled in red for 10000 samples at the centre of the jet where exit velocity is maximum.

## 4. Conclusion and Future Work

In conclusion, this comprehensive analysis of characterising turbulent flows from a single circular jet using PIV sheds light on the intricate dynamics influencing fluid behaviour. The experimental setup was done in a low-speed recirculating water tunnel and captured tracing particles illuminated by a laser using a high-speed camera. The utilisation of PIV, a non-intrusive technique, enabled the collection of precise velocity field data crucial for the analysis.

The results revealed the evolution of flow patterns at certain points downstream, with the mean streamwise velocity experiencing decay and gradual dissipation of kinetic energy. The examination of the Reynolds shear stress provided insights into momentum distribution between fluid layers, specifically highlighting the instabilities caused by the shear layer. Vorticity patterns showed the dynamic behaviour of fluid flow and the susceptibility to instabilities. The TKE was a key parameter in quantifying the chaotic fluid motion, showing higher turbulence levels in shear layer regions.

The uncertainty analysis acknowledged potential errors in the experiment setup and recording process.

This investigation could have been extended to explore the impact of varying jet diameter and Reynolds number, on the observed turbulent characteristics. Advanced analysis of using frequency and proper orthogonal decomposition (POD) could complement experimental findings and provide a more comprehensive understanding of fluid dynamics.

This report contributes to the ever-expanding research on turbulent flow dynamics and knowledge that will offer valuable insights for future engineering applications and design considerations.

## 5. References


[1] Abdel-Rahman, A.A., Al-Fahed, S.F. and Chakroun, W. (1996) 'The near-field characteristics of circular jets at low Reynolds numbers', *Mechanics Research Communications*, 23(3), pp. 313–324. Available at: https://doi.org/10.1016/0093-6413(96)00028-6.

[2] Becker, H.A. and Massaro, T.A. (2068) 'Vortex evolution in a round jet', *J. Fluid Me&*, 31, pp. 435–448. Available at: https://doi.org/10.1017/S0022112068000248.

[3] Bradshaw, P. (2066) 'The effect of initial conditions on the development of a free shear layer'. Available at: https://doi.org/10.1017/S0022112066001204.

[4] Crow, S.C. and Champagne, F.H. (2071) 'Orderly structure in jet turbulence Introduction Flow-visualization experiments Means of forcing the jet Structure of the preferred mode Amplitude response at various Strouhal numbers Axial profiles at various Strouhal numbers Summary description of the modes Influence of forcing on entrainment and background turbulence Comparison with stability theory Concluding remarks', *J. Fluid Mech*, 48, pp. 547–591. Available at: https://doi.org/10.1017/S0022112071001745.

[5] Fellouah, H., Ball, C.G. and Pollard, A. (2009) 'Reynolds number effects within the development region of a turbulent round free jet', *International Journal of Heat and Mass Transfer*, 52(17–18), pp. 3943–3954. Available at: https://doi.org/10.1016/J.IJHEATMASSTRANSFER.2009.03.029.

[6] Gohil, T.B., Saha, A.K. and Muralidhar, K. (2012) 'Numerical study of instability mechanisms in a circular jet at low Reynolds numbers', *Computers & Fluids*, 64, pp. 1–18. Available at: https://doi.org/10.1016/J.COMPFLUID.2012.04.016.

[7] Hyun, B.-S., Balachandar, R. and Yu, K. (2014) 'PIV/LDV MEASUREMENTS OF MEAN VELOCITY AND TURBULENCE IN A COMPLEX OPEN CHANNEL FLOW'. Available at: https://www.researchgate.net/publication/255590049 (Accessed: 17 December 2023).

[8] Keane, R.D. and Adrian, R.J. (1992) 'Theory of cross-correlation analysis of PIV images', *Applied Scientific Research*, 49, pp. 191–215.

[9] Olsson, M., Fuchs, ; L and Fuchs, L. (1996) 'Large eddy simulation of the proximal region of a spatially developing circular jet', *Physics of Fluids*, 8, pp. 2125–2137. Available at: https://doi.org/10.1063/1.868987.

[10] Raffel, M. *et al.* (2018) 'PIV Uncertainty and Measurement Accuracy', *Particle Image Velocimetry*, pp. 203–241. Available at: https://doi.org/10.1007/978-3-319-68852-7_6.

[11] 'Reynolds number effects on the behavior of a non-buoyant round jet' (no date). Available at: https://doi.org/10.1007/s00348-005-0976-6.

[12] Rovira, M., Engvall, K. and Duwig, C. (2020) 'Review and numerical investigation of the mean flow features of a round turbulent jet in counterflow', *Physics of Fluids*, 32(4), p. 45102. Available at: https://doi.org/10.1063/5.0003239/1080526.

[13] Shashi Menon, E. (2015) 'Fluid Flow in Pipes', *Transmission Pipeline Calculations and Simulations Manual*, pp. 149–234. Available at: https://doi.org/10.1016/B978-1-85617-830-3.00005-5.

[14] Z A M A N And, K.B.M.Q. (2080) 'Vortex pairing in a circular jet under controlled excitation. Part 1. General jet response', *J. Fluid Me&*, 101, pp. 449–491. Available at: https://doi.org/10.1017/S0022112080001760.

[15] Zang, B. and New, T.H. (2015) 'On the wake-like vortical arrangement and behaviour associated with twin jets in close proximity', *Experimental Thermal and Fluid Science*, 69, pp. 127–140. Available at: https://doi.org/10.1016/J.EXPTHERMFLUSCI.2015.08.004.